Mechanics of Materials 191 (2024) 104944

Contents lists available at ScienceDirect

Mechanics of Materials

journal homepage: www.elsevier.com/locate/mechmat

Research paper

The coupled effect of aspect ratio and strut micro-deformation mode on the mechanical properties of lattice structures

Stylianos Kechagias **, Kabelan J. Karunaseelan, Reece N. Oosterbeek, Jonathan R.T. Jeffers *

Department of Mechanical Engineering, Imperial College London, London, SW7 2AZ, United Kingdom

ARTICLE INFO

Keywords:
Lattice structures
Additive manufacturing
Bend-dominated
Stretch-dominated
Height-to-diameter ratio
Height-to-width ratio

ABSTRACT

Lattice structures have been integrated into various industrial applications owing to their unique compressive properties. Mechanical characterisation is usually done by testing a small specimen which is assumed representative of the utilised lattice. A specimen's aspect ratio (height to diameter/width ratio) is known to affect compressive properties in various engineering materials, yet its influence in lattices has not been investigated thoroughly. In this study, titanium lattice specimens designed with different aspect ratios (ranging from 0.5 to 3.0) and four different topologies (displaying bend and stretch-dominated micro-deformation modes) were fabricated using powder bed fusion and tested in quasi-static compression. Their compressive properties and failure modes were evaluated using acquired stress-strain curves and digital image correlation (DIC) analysis. Reducing the aspect ratio in the bend-dominated lattices increased the measured stiffness of the specimens by up to 40%. Conversely, increasing the aspect ratio of the stretch dominated lattices increased the measured stiffness of the specimens by up to 30%. For both topology types, decreasing the aspect ratio increased the measured strength of the specimens, but the effect was less than that observed for stiffness. Different responses were attributed to gradient strain accumulation and different failure patterns (densification versus shear banding) that were observed depending on the combination of aspect ratio and topology. These findings are particularly important for better predicting the mechanical behaviour of lattice-based components that have aspect ratios outside the range of conventional test specimens.

1. Introduction

Lattice structures are used in various industrial applications, in particular load-bearing applications like sandwich panels with high specific strength, dampers with high energy absorption and orthopaedic implants with stiffness matched to natural bone (Maconachie et al., 2019; Findeisen et al., 2017; Zadpoor, 2019). It is important that in such applications the mechanical properties of the lattice are well characterised. However, a problem arises because (a) we know that the measured mechanical properties of a lattice depend on the aspect ratio of the specimen being tested and (b) the aspect ratio of the applications above can be wholly different to the standardised aspect ratio of test specimens used to characterise the lattice's mechanical properties. A further challenge arises due to the paucity of data on how topology interacts with aspect ratio to affect the lattice's mechanical properties.

International testing standards (such as the ISO 13314 and ASTM D1621) are based on the idea that mechanical testing of a small specimen of a lattice is representative of the structure when deployed in an application. The standards require specimens to be adequately large (consisting of at least 10 unit cells across the width to avoid size effects) with an aspect ratio (specimen height to diameter/width ratio, $\zeta = H/D$ or H/W) between 1 and 2 (International Organization for Standardization, 2011;American Society for Testing and Materials, 2000). The effect of aspect ratio in cellular materials has primarily been investigated for the uniaxial compression of trabecular bone cores. Linde et al. (1992) showed that increasing the aspect ratio of the test specimen increased the measured stiffness. The same trend for stiffness was found by Ang et al. (2012) who further showed that increasing the aspect ratio of the test specimen reduced the measured ultimate strength. These studies, however, employed specimens with relatively small sizes making them prone to size effects due to structural artefacts (Keaveny et al., 1993).

Limited data exists for man-made lattices and conclusions are contradictory. In sandwich panel structures, increasing the aspect ratio was reported to reduce the measured modulus and strength (Zupan et al.,

* Corresponding author.
** Corresponding author.
E-mail addresses: s.kechagias20@imperial.ac.uk (S. Kechagias), j.jeffers@imperial.ac.uk (J.R.T. Jeffers).

https://doi.org/10.1016/j.mechmat.2024.104944
Received 20 June 2023; Received in revised form 16 December 2023; Accepted 4 February 2024
Available online 12 February 2024

2004). However, in polymeric foams, increasing the aspect ratio was reported to increase the measured modulus but conversely decrease the measured strength (Thomson et al., 1995). In magnesium foams, increasing the aspect ratio was also reported to reduce the strength (Xia et al., 2012). Other works in periodic lattices demonstrate either increasing (Contreras Raggio et al., 2022) or decreasing (Peng et al., 2022) modulus for increasing aspect ratio. Still, specimens in these works consisted of few layers and cells, hence it was not clear whether the stiffening effect originated from the aspect ratio or edge/size effects (Yoder et al., 2018; Pham and Hütter, 2021). Interesting findings from numerical studies of periodic lattices report that altering aspect ratio results in different strain distributions inside the structures (Yang et al., 2019; Zhang et al., 2022; Bühring et al., 2022) suggesting it may have an effect on the measured properties of the structure.

All the above indicate that the aspect ratio and topology of a test specimen affects its measured mechanical properties, and that strain fields inside the lattice change depending on aspect ratio. Nevertheless, it is well-known that topology dictates the developed strain fields in a lattice through struts' micro-deformation mode and internal loading state. Under external compression, struts can either bend or carry axial loads making the structure more compliant (bend-dominated) or very rigid (stretch-dominated). This classification is usually done through the Maxwell criterion by parallelising a lattice to either an indeterminate frame (stretch-dominated) or a pin-joined mechanism (bend-dominated) (Ashby, 2006; Deshpande et al., 2001).

A better understanding on how aspect ratio and bend/stretch-domination affect the properties of a lattice is still needed. This is important to consider when the application requires lattice structures with aspect ratios out of the bounds of standardised testing specimens. Of particular interest are fully porous orthopaedic implants designed to locally match the properties of natural bone, and implants can potentially have high aspect ratios (e.g., femoral stems) or low aspect ratios (e.g., knee replacement components) (Cortis et al., 2022; Burge et al., 2023). Other applications that require precisely controlled lattice structures at different aspect ratios are shock absorber and dampers (Yang and Ma, 2019). Understanding the effect of macroscopic aspect ratio can lead to better design of mechanical metamaterials for energy absorption applications. Moreover, functionally graded structures to induce locally varied deformation behaviours could be designed by stacking topologies of different aspect ratios – alternatively to previous concepts where only unit cell size or topology were varied (Liu et al., 2018; Vangelatos et al., 2020; Lei et al., 2021).

The aim of this study is to measure the mechanical properties of lattice structures with aspect ratios that are representative of their application in stretch and bend dominated forms. These data should elucidate how aspect ratio and topology affect the measured mechanical properties, providing a useful tool to engineers seeking to deploy lattice structures in a variety of applications.

2. Materials and methods

2.1. Specimen design

Four lattice topologies of specimen were included in the study: a stretch-dominated (high connectivity) stochastic lattice, a bend-dominated (low connectivity) stochastic lattice (Kechagias et al., 2022), a bend-dominated body-centred cubic (BCC) lattice (Leary et al., 2018) and a stretch-dominated octet-truss lattice (Qi et al., 2019). Specimens were designed as line geometries using Rhinoceros 7 (Robert McNeel & Associates, USA) with the 7 aspect ratios of comparable volumes as shown in Table 1.

The stochastic lattices were generated by populating cylindrical volumes with pseudo-randomly distributed points which were joined to produce specimens with fixed strut density (struts per volume) and connectivity (Z). A connectivity of 8 was used to produce the stretch-dominated (Z8) stochastic lattices and a connectivity of 4 was used to produce the bend-dominated (Z4) stochastic lattices as described in (Kechagias et al., 2022).

Table 1
Nominal dimensions of tested specimens.

Aspect ratio ζ	Height to diameter/width ratio (H/D or H/W) [mm/mm]					
	BCC (l = 1 mm)	BCC (l = 1.5 mm)	BCC (l = 2 mm)	Stochastic Z4	Stochastic Z8	Octet-truss
0.50	13/26	19.5/39	26/52	13/26	13/26	13/26
0.65	13/20	–	–	–	13/20	–
1.00	13/13	–	–	–	13/13	–
1.60 or 1.62	21/13	31.5/19.5	32/20	21/13	21/13	20.8/13
2.00	26/13	–	–	–	26/13	–
2.54	33/13	–	–	–	33/13	–
3.00	39/13	58.5/19.5	60/20	39/13	39/13	39/13

The periodic lattices were designed as square prisms consisting of the BCC or the octet-truss unit cells. In both periodic lattices, the unit cells were cubic with edge length l equal to 1, 1.5 or 2 mm for the BCC, and 1.3 mm for the octet-truss. A minimum of 13 and 10 unit cells were used to form the edges of the BCC and octet-truss lattices, respectively. Specimen dimensions used for each lattice type are also included in Table 1.

The angle of struts with respect to the build plate (XY plane) was equal to 35.3° in the BCC lattices, and 0° and 45° in the octet-truss lattices. The stochastic lattices had struts in all directions, with fixed distribution of angles between the struts and the XY plane. Struts with an angle <25° were designed with a kink in the middle to assure printability (Hossain et al., 2021).

2.2. Specimen manufacturing

The line geometries were sliced using a customised software which allocates bespoke laser parameters to each line to produce a uniform strut thickness as described in (Kechagias et al., 2022; Ghouse et al., 2017). Lattice specimens were fabricated using a powder bed fusion system (AM250, Renishaw, UK) and commercially pure titanium (Grade 2, Ø10–45 μm, D50: 32.4 μm). Struts were produced by hatching the contour of their projection slices using a 70 μm laser spot diameter, 50 W laser power, and 50 μm layer thickness. Laser exposure was varied depending on strut angle in respect to the build plate as shown in Table S1 in Supplementary materials.

A total of 156 specimens were fabricated for this study. Specimens of same lattice type were printed in the same batches so that they would not to be affected by the degree of powder recycling (Guo et al., 2021). All specimens were printed vertically with supports only at the bottom surface to eliminate the effect of printing angle (Pehlivan et al., 2020) when comparing specimens of same type. After printing, specimens were trimmed from the build plate by electro discharge machining, loading surfaces were ground parallel and cleaned ultrasonically with acetone. The relative density of each specimen was calculated by dividing the apparent density ρ (measured mass to volume ratio) to the density of solid titanium (ρ_s = 4.51 g/cm^3).

2.3. Lattice imaging and characterisation

One specimen per type was micro-CT scanned with a Zeiss Xradia 510 Versa (Carl Zeiss AG, Germany). Scans were performed at 80 kV using 2401 projections, 5 s exposure time and a pixel size of 12 μm. Using the reconstructed scan data, the mean pore size (taken as the trabeculae separation) and the enclosed porosity for each lattice type were measured using CTAn (Bruker Ltd., United Kingdom) (Hildebrand and Ruegsegger, 1997). In addition, using the micro-CT data of each lattice type, the open-source software StrutSurf (Oosterbeek and Jeffers, 2022) was used to assess the strut thickness (i.e., strut diameter) and the

arithmetic mean surface roughness of struts built at different angles.

Additionally, one specimen per type was imaged using scanning electron microscope (Mira, TESCAN, Czech Republic) to evaluate the quality of the additively manufactured specimens. Images were taken using 5 keV and 1 nA.

2.4. Quasi-static compression testing

Mechanical compression tests were performed using universal testing machines (Instron 5565 and 8872) in line with ISO 13314:2011 (International Organization for Standardization, 2011). Load was recorded using load cells (load cell capacities: 5 kN, 10 kN and 25 kN) and displacement was recorded using two linear variable differential transformers attached to the moving platen (data acquisition rate was kept constant at 15 Hz). Stress-strain curves were then produced using the nominal stress and nominal strain.

Compression was carried out in quasi-static conditions with constant strain rate of 0.0016 s^{-1}; hence platen's displacement rate was adjusted to each specimen's height. A pilot specimen was used to estimate the plateau stress of each design (average recorded stress between 20% and 30% strain). Accurate mechanical characterisation was performed by compressing specimens (n = 5 per design) to 35% strain. From the acquired data (see examples in Fig. 1), the elastic modulus E (assumed equivalent to structure's stiffness) was taken equal to the slope of a pre-yield hysteresis loop (upper and lower bound 70% and 20% of plateau stress respectively). Yield stress was estimated using the 0.2% plastic strain offset. The first maximum stress (or in case of no distinguishable local maximum, the stress at 1% plastic strain offset from the hysteresis loop) were taken as the (ultimate) compressive strength. Lastly, the energy absorption was calculated as the area under the stress-strain curve up to 30% strain, excluding the hysteresis loop. Energy absorption was only calculated for bend-dominated lattices as only these are used for energy absorption applications since they do not exhibit stress softening or shear band fracture after yield.

Testing was structured to firstly identify the effect of aspect ratio on the stretch dominated stochastic and bend dominated BCC structures. Secondly a reduced set of compression tests were performed on the stretch-dominated octet-truss and the bend-dominated stochastic structures to confirm the results were not limited to specific lattice topologies. And lastly, two extra bend-dominated BCC structures with lower relative density to investigate whether the effect of aspect ratio is independent to relative density.

2.5. Statistical analysis

Firstly, the effect of aspect ratio in the mechanical properties of each topology was investigated through one-way analysis of variance (ANOVA). Tukey's *post hoc* test was then used to group aspect ratios that did not differ significantly. Secondly, a 2-way ANOVA was used to compare the mechanical properties among the BCC lattices built with different aspect ratios and unit cell sizes (i.e., unit cell edge length), followed by Tukey's post hoc test to see the effect of aspect ratio and unit cell size. Thirdly, a 1-way ANOVA was used to compare the measured strut thickness and strut roughness at different build angles across all imaged samples (one per type).

Statistical analysis was performed in GraphPad Prism (GraphPad Software, Inc., USA) and a $p < 0.05$ was considered indicative of significant difference. Data are presented as mean ± SD for n = 5. In figures, (*) indicates $p < 0.05$, (**) indicates $p < 0.01$, (***) indicates $p < 0.001$, and no notation indicates groups with no significantly different values ($p > 0.05$).

2.6. Digital image correlation analysis

Digital image correlation (DIC) was used to measure the full field planar strain distribution of the lattice structures during compression. A digital camera (1080p resolution, 30 fps, 750D Canon, Japan) positioned normal to the lattice structures recorded the loading operation from intact to deformed states. Each video was post processed in 2-D DIC software (GOM Correlate Professional, Germany). A facet size of 19 pixels and 50% overlap was used throughout to track the visible strut features of the lattice structures. The field of view was adjusted so that strut features had a size of 3–5 pixels, to minimize aliasing and degrading spatial resolution during compression testing. The (%) longitudinal strain ε_z defined as the strain in the loading direction was used to assess the influence of topology and aspect ratio of the lattice structures.

3. Results

3.1. Lattice characteristics

Key structural characteristics for each lattice type are summarised in Table 2. Specimens' dimensions exhibited high consistency with less than 2% deviation from nominal values. Furthermore, according to established guidelines (International Organization for Standardization,

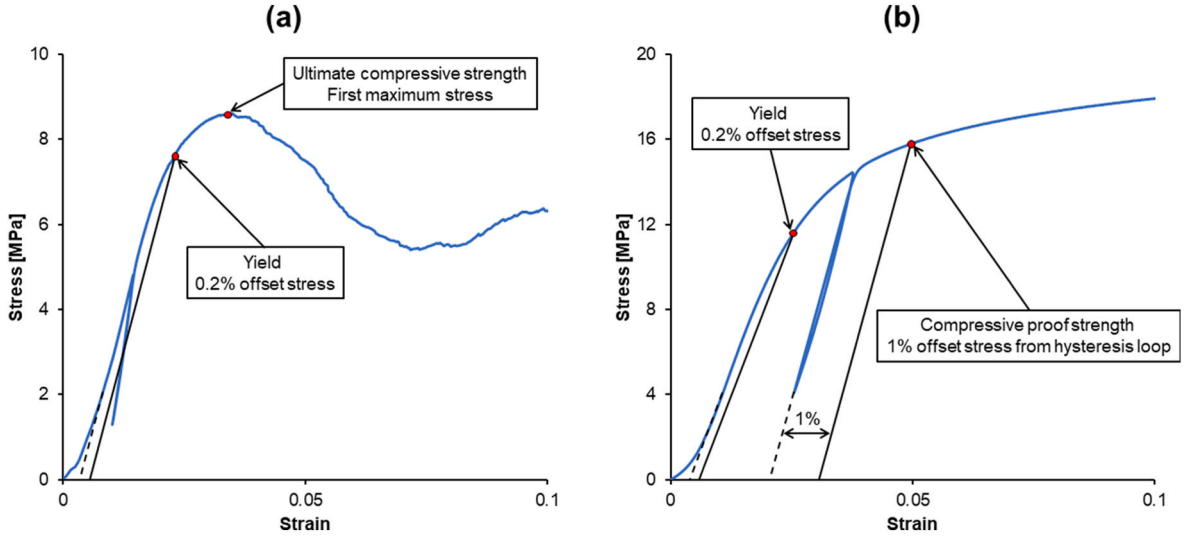

Fig. 1. Representative stress-strain curves (up to 10% strain). Depending on lattice type, specimens can exhibit (a) a local maximum stress or (b) post-yielding plateau stress.

Table 2
Structural characteristics of each lattice type.

Characteristic	BCC	BCC	BCC	Stochastic	Stochastic	Octet-truss
Connectivity [struts/node]	8	8	8	4	8	12
Unit cell size l [mm]	1.0	1.5	2.0	–	–	1.3
Strut density [struts/mm^3]	8.0	2.4	1.0	3.0	3.0	11.0
Strut thickness/length t/L	0.27	0.17	0.13	0.23	0.18	0.25
Micro-deformation mode	Bending	Bending	Bending	Bending	Stretching	Stretching
Relative density [%]	20.1 ± 0.4	9.8 ± 0.3	5.8 ± 0.2	9.0 ± 0.2	11.5 ± 0.3	30.6 ± 0.3
Pore size [mm]	0.51 ± 0.10	0.86 ± 0.16	1.30 ± 0.19	1.03 ± 0.27	0.96 ± 0.34	0.45 ± 0.18

2011; Tekoglu et al., 2011; Andrews et al., 2001), specimens would not be expected to encounter size effects, as the minimum dimension used (13 mm) was more than 10 times larger than the average pore measured in all lattice types.

All topologies were fabricated with minimal structural defects with representative images shown in Fig. 2. Typical forms of surface roughness associated with powder bed fusion, such as semi-sintered particles and strut waviness, were seen in all specimens. Struts' arithmetic mean surface roughness ranged from 5 to 20 μm with the low-angled struts (<30°) demonstrating higher roughness (see Figure S1 in Supplementary Materials). Yet, strut thickness was found to be consistent and equal to ≈230 μm among all topologies and build angles as aimed ($p > 0.05$, see Figure S1 in Supplementary Materials). In addition, enclosed porosity was found to be <0.01% in all specimens. This data is in line with previous results (Kechagias et al., 2022; Ghouse et al., 2017; Oosterbeek and Jeffers, 2022) and suggest that the manufacturing process exhibited high consistency and repeatability for the fabrication of all lattice types.

3.2. Convergence analysis for aspect ratio on stretch and bend dominated lattices

Measured stiffness, strength and energy absorption values are summarised in Figs. 3 and 4, respectively. The aspect ratio had strong effect ($p < 0.001$) on each mechanical property (stiffness, yield, ultimate compressive strength, and energy absorption). The stochastic (stretch-dominated) lattices (see Fig. 3a) demonstrated constant stiffness for $\zeta \leq 2$ ($p > 0.05$) and increased stiffness for larger aspect ratios ($p < 0.05$). On the contrary, the BCC (bend-dominated) lattices (see Fig. 3b) demonstrated constant stiffness for $\zeta > 1$ ($p > 0.05$) and increased stiffness for smaller aspect ratios ($p < 0.05$).

The stochastic and BCC lattices exhibited similar trends regarding yield (Fig. 4a) and compressive strength (Fig. 4b). The yield and compressive strength of the stochastic (stretch-dominated) lattice reduced as ζ increased from 0.5 to 0.65 ($p < 0.01$), but thereafter remained constant as ζ increased to 3. The yield and compressive strength of the BCC (bend-dominated) lattice reduced as ζ increased from 0.5 to 1 ($p < 0.01$), but thereafter also remained constant as ζ increased to 3. The effect of aspect ratio on strength was small (13% for the stochastic and 20% for the BCC lattices) compared to its effect on stiffness (29% for the stochastic and 40% for the BCC).

For the BCC (bend-dominated) structures, the energy absorption reduced as the aspect ratio increased from 0.5 to 1 ($p < 0.01$), but thereafter remained the same ($p > 0.05$) (Fig. 9). The higher energy absorption was related to the higher plateau stress (equivalent to the measured compressive strength) in the lower aspect ratio specimens.

Representative stress-strain curves and DIC images from the quasi-static compression tests are displayed in Fig. 5. The shapes of the curves resembled well-known patterns that are associated with stretch and bend-dominated response of lattices in the micro-scale (Ashby, 2006). In stochastic (stretch-dominated) lattices, stress reached a peak value which was followed by stress softening owing to the localised fracture of cells through the formation of shear bands, ultimately leading to catastrophic failure. On the contrary, cells in BCC (bend-dominated) lattices tend to collapse, and structures fail in a layer-by-layer manner due to the bending of their struts, ultimately leading to structure

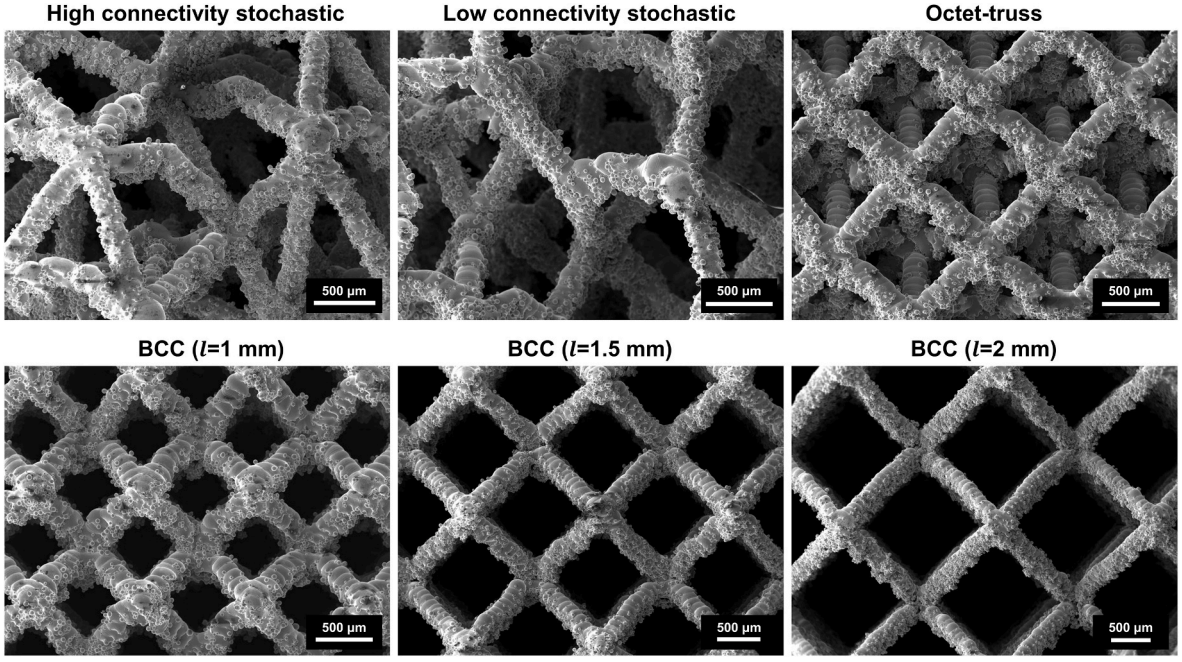

Fig. 2. Scanning electron microscopy images of fabricated specimens for each lattice type.

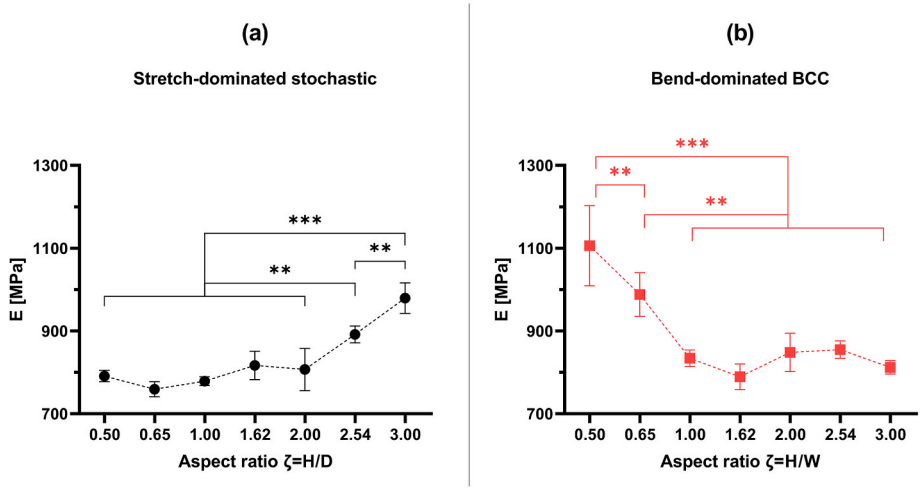

Fig. 3. The elastic modulus E (equivalent to structures' stiffness) for different aspect ratios of (a) stochastic and (b) BCC lattices. Statistical results are summarised with more detail in Tables S2 and S3 in Supplementary materials.

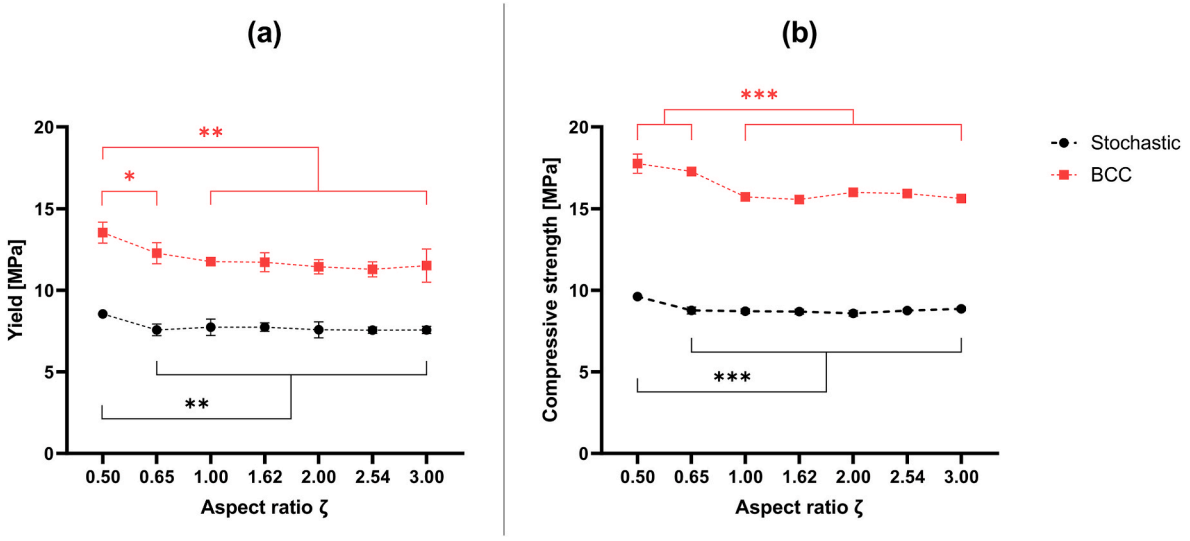

Fig. 4. The (a) yield and (b) ultimate compressive strength for different aspect ratios of the stretch-dominated stochastic and the bend-dominated BCC lattices. No comparison between lattice types was performed. Statistical results are summarised with more detail in Tables S4–S7 in Supplementary materials.

densification.

For the stochastic (stretch-dominated) lattices with the smallest aspect ratio ($\zeta = 0.5$), multiple shear bands were observed which increased the measured strength of the specimen, but not its measured stiffness. Post yield, the stress-strain curves demonstrated relatively low stress fluctuation indicating that locally collapsed regions did not merge to a catastrophic crack (as seen in Fig. 5). High aspect ratio specimens (ζ equal to 2.54 and 3) progressively compressed due to the generation of multiple distinct shear bands; a major shear band was followed by secondary ones generated at distant regions along specimens' height. This did not affect the specimen's measured strength but did increase the measured stiffness (Figs. 3 and 4).

For the BCC (bend-dominated) lattices, high strain accumulated centrally in the low aspect ratio BCC specimens (ζ equal to 0.5 and 0.65), while the sides of the specimen experienced less strain. High stain accumulation near the platens corresponded to the collapse of cell rows in the vicinity of platens which further disrupted stress distribution towards the centre. This had the effect of increasing the measured stiffness, strength (Fig. 4) and energy absorption of the specimen (Fig. 9). The intermediate aspect ratio specimens ($1 \leq \zeta \leq 2$) exhibited uniform strain accumulation along specimen's height and a macroscopic barrel shape at failure, while the high aspect ratio specimens ($\zeta > 2$) exhibited macroscopic (global) buckling behaviour with localised strains forming two symmetrical shear bands about specimen's mid-plane. However, these phenomena for the intermediate and large aspect ratio did not affect the measured mechanical properties.

3.3. *The role of micro-deformation mode*

Representative stress-strain curves of the stretch dominated octet-truss lattices (Fig. 6a) and the bend-dominated Z4 stochastic lattices (Fig. 6b) confirm that the observations in **3.2** were not confined to particular lattice topologies. The shape of the curves as well as the failure mode of the specimens were unaffected by altering aspect ratio in both cases.

In the octet-truss lattices, a major diagonal shear band generated a cleavage line leading to catastrophic failure in the intermediate and high aspect ratio specimens, making the structures appear more brittle (Fig. 6a). In the low aspect ratio specimens, multiple shear bands at distant regions were formed which did not lead to catastrophic fracture,

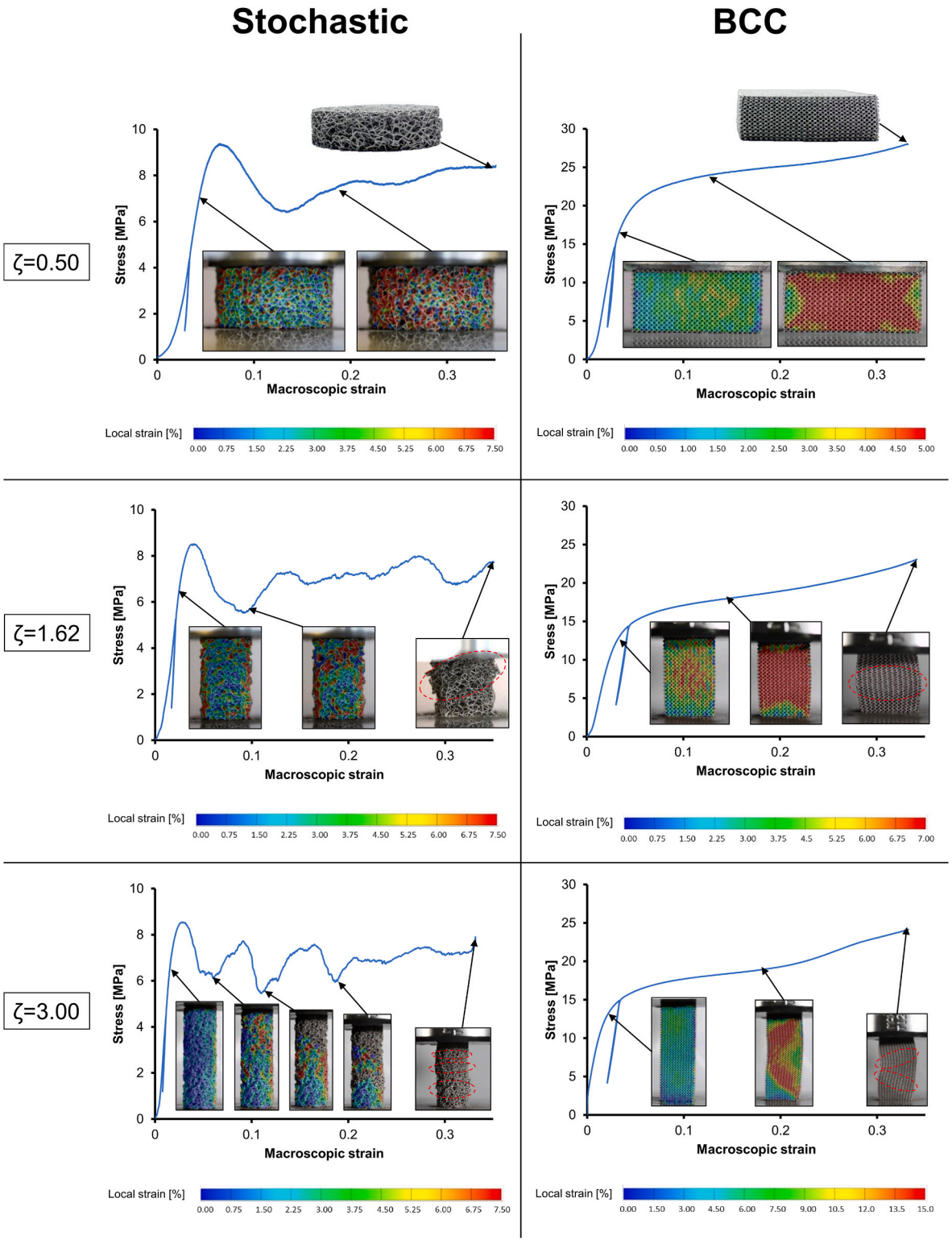

Fig. 5. Stress-Strain curves for stochastic (stretch-dominated) and BCC (bend-dominated) structures with aspect ratio of 0.5, 1.62 and 3.0. Embedded DIC images capture the local longitudinal stains at the point of yield and at the plastic deformation region. A longitudinal strain scale is provided for each specimen. Circles indicate the fracture regions in the plain images at end point of tests.

caused a smaller post-yield stress drop and made the lattices appear more ductile (Fig. 6a).

In the Z4 stochastic lattices, the $\zeta = 0.5$ and $\zeta = 1.62$ aspect ratio specimens exhibited collapsed towards the middle of the specimen (Fig. 6b) as previously seen in low connectivity structures such as lattices, foams and trabecular bone cores (Kechagias et al., 2022; Vesenjak et al., 2012; Nazarian et al., 2005). More interestingly though, the high aspect ratio ($\zeta = 3$) specimens demonstrated a macroscopic buckling which originated by the collapse of two main regions along specimen's length (Fig. 6b). These observations matched the ones seen previously in the bend-dominated BCC lattices.

When considering the measured mechanical properties, similarly to

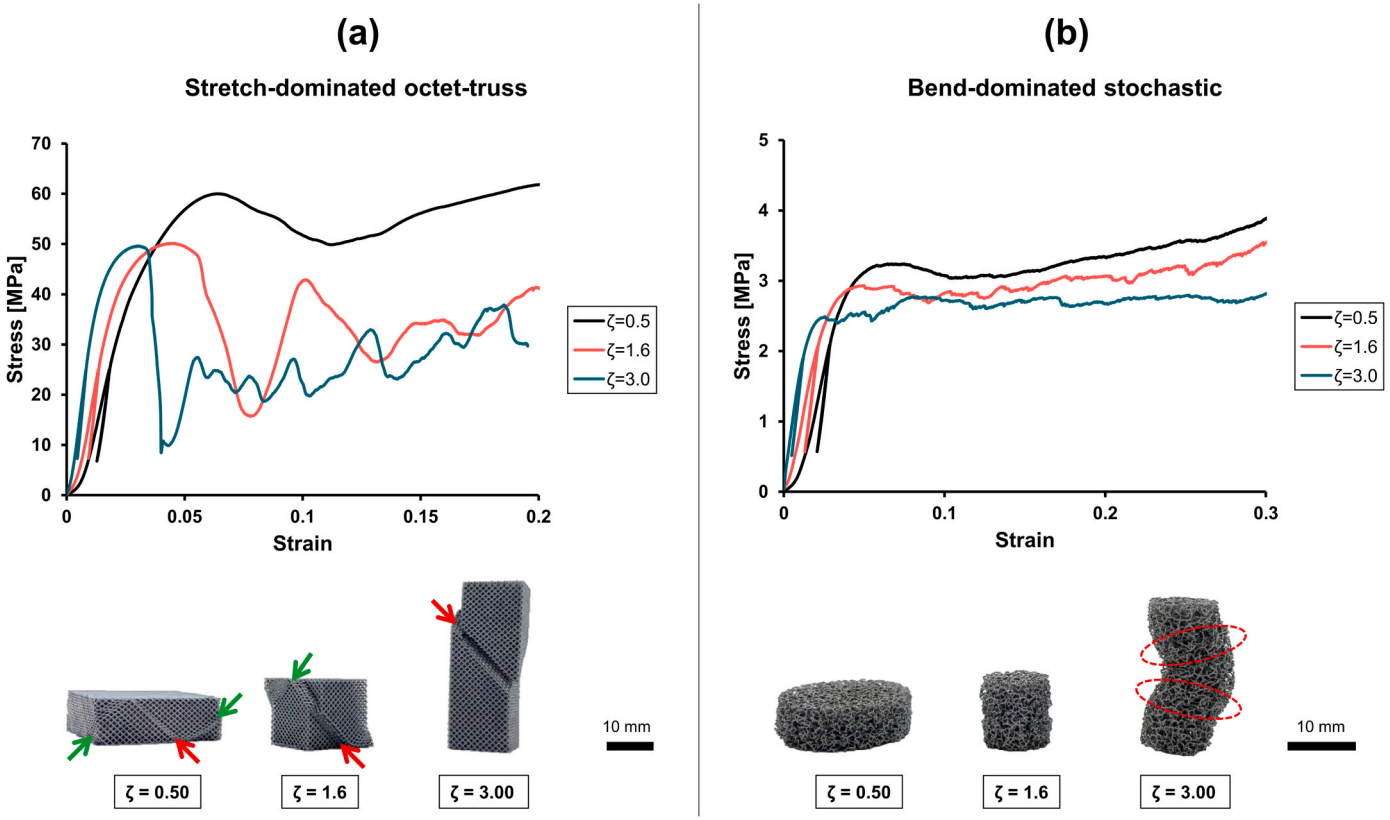

Fig. 6. Representative stress-strain curves of (a) the stretch-dominated octet-truss lattices and (b) the bend-dominated Z4 stochastic lattices. Embedded images demonstrate failed specimens; red and green arrows indicate major and any secondary shear bands generated inside the octet-truss specimens. Circled regions in the stochastic lattice with $\zeta = 3$ indicate local collapses that led to macroscopic buckling. (For interpretation of the references to colour in this figure legend, the reader is referred to the Web version of this article.)

the stretch-dominated (Z8) stochastic lattices, the stiffness of the octet-truss lattices increased with increasing aspect ratio (Fig. 7a). While, similarly to the bend-dominated BBC lattices, the stiffness of the bend-dominated (Z4) stochastic lattices increased with decreasing aspect ratio (Fig. 7b). In both cases, the ultimate strength decreased with increasing aspect ratio. Although the trends in stiffness and strength were the same for fixed micro-deformation mode (stretch-dominated and bend-dominated structures), the change in properties happened at different values of aspect ratio indicating that each individual topology may display different convergence threshold.

3.4. The role of relative density

Two additional (highly porous) BCC lattice structures with relative densities of 6% and 10% were tested. Both structures demonstrated similar shapes of stress-strain curves with the BCC lattice tested in **section 3.2** (relative density 20%). Representative curves for three different aspect ratios (ζ equal to 0.5, 1.6 and 3.0) are shown in the Supplementary Figure S2 in the Supplementary Materials. In addition, both types of the highly porous BCC lattices demonstrated similar macroscopic failure patterns with the BCC specimens tested in **3.2**. In particular, the high aspect ratio specimens ($\zeta = 3.0$) exhibited two main regions of high localised densification which led to macroscopic buckling (Fig. 8). The specimens with the intermediate aspect ratio ($\zeta = 1.6$) exhibited a uniform densification towards the middle of the structure (Fig. 8). While the low aspect ratio specimens ($\zeta = 0.5$) exhibited highly gradient local deformation at two sides of the specimen. One side displayed a collapse at the site of the moving platen while the other side generated a shear band collapse. The generation of shear bands in the BCC lattices has previously linked to low relative densities and the resultant low strut thickness-to-length ratios (slender struts with t/L close to 0.1) (Gümrük and Mines, 2013).

While these observations are highly in line with the ones seen at the BCC of **section 3.2**, the effect of aspect ratio in the mechanical properties was seen to decline with decreasing relative density (Fig. 9). Similar to all previously tested structures, compressive strength was found to increase at lowest aspect ratio tested ($\zeta = 0.5$) for both highly porous BCC lattices (11% increase when $l = 1.5$ mm and 8% increase when $l = 2$ mm). Furthermore, the BCC lattice with 10% relative density exhibited a similar trend of increasing stiffness and energy absorption with decreasing aspect ratio as seen in the BCC lattice with 20% relative density. On the contrary, no statistical difference was seen on the stiffness and energy absorption of the BCC with 6% relative density for different aspect ratios.

Overall, statistical analysis revealed that aspect ratio and relative density had a coupled effect on all mechanical properties that were investigated ($p < 0.001$ for the interaction in Tables S12–S14 in the Supplementary Materials).

4. Discussion

The most important finding of this study is the aspect ratio and topology of a lattice structure test specimen affects the measured mechanical properties and failure mechanisms. Increasing aspect ratio increases the measured modulus for stretch-dominated topologies but decreased the modulus for bend-dominated topologies. To a lesser extent, the aspect ratio also affected a specimen's measured strength, which decreased as the aspect ratio increased for both stretch and bend dominated topologies. The reason for these findings is the number and location of strain shear bands that form within the specimen under load which depends on (a) the aspect ratio and (b) whether the specimen's topology is stretch or bend dominated. These findings are important

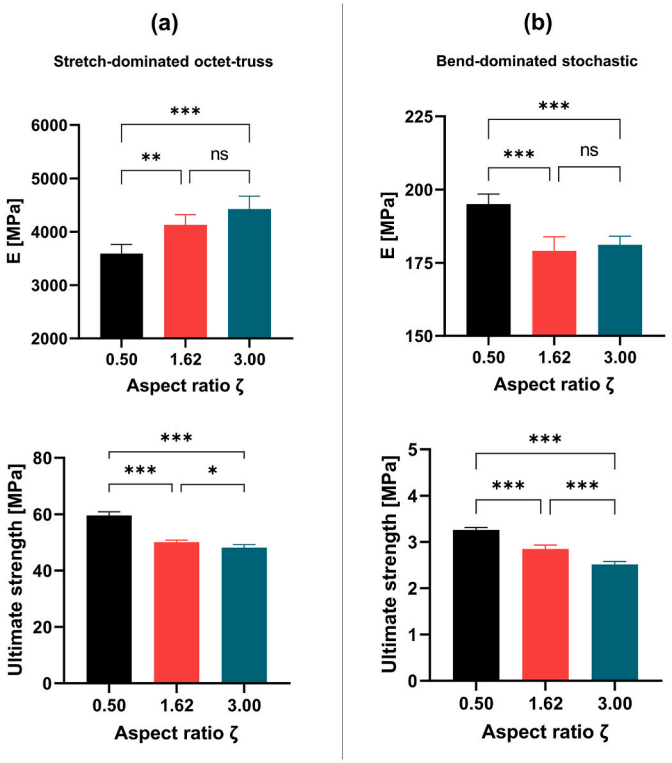

Fig. 7. Measurements of the elastic modulus E and ultimate compressive strength for different aspect ratios for (a) the stretch-dominated octet-truss lattices and (b) the bend-dominated Z4 stochastic lattices. Statistical results are summarised with more detail in Tables S8-S11 in Supplementary materials.

because many engineering components necessarily have aspect ratios outside the bounds of standards such as ISO 13314 and ASTM D1621. In these cases, it is critical to understand how properties and failure mechanisms of the in-situ component may deviate from the standardised test specimen geometry.

4.1. Results interpretation

For the bend-dominated BCC structures, failure patterns and strain accumulation captured through DIC highly aligns with previous experimental (Leary et al., 2018; Gümrük and Mines, 2013) and numeral models (Yang et al., 2019). Numerical studies on sandwich BCC lattices of different aspect ratio have shown that structure's macro-stiffness is affected by local stiffness gradients due to the confined cells' deformation (Yang et al., 2019). In our study, the boundaries of the lattices were free and the stiffening of BCC lattices with decreasing aspect ratio was linked to end-induced stress concentrations, caused by collapse of cells near the platens which generated high friction. This becomes more pronounced with increasing cross-sectional area (Linde et al., 1992). This only applied to BCC specimens with aspect ratio <1. BCC specimens with larger aspect ratio were not disrupted by end-effects or buckling and the measured stiffness remained constant.

For the stretch-dominated stochastic structures, there was no stiffening of the specimen at smaller aspect ratios. This was because the cells near the platens did not collapse since their nodes are more tightly interconnected and the specimen behaves more like an indeterminate frame structure (Ashby, 2006). However, the stretch dominated structures exhibited stiffening at higher aspect ratios. This was considered to be caused by the formation of incremental distortion resulting in localised deformation bands well before the collapse point – this has been observed previously for foams (Ashby et al., 2001) and in numerical models for lattices (Bühring et al., 2022). The apparent increase in stiffness may have then been due to a larger portion of the specimen height remaining intact after cells' initial distortion in the quasi-elastic region, making the structure more resistant to further deformation.

By testing two extra topologies: a bend-dominated stochastic structure and a stretch-dominated octet-truss structure, it was verified that the above stiffening mechanisms as well as the macroscopic failure modes observed were not topology-dependent but rather highly associated with the intrinsic micro-deformation mode of each structure (bend-dominated versus stretch-dominated). Additionally, the experimental observations regarding the failure mechanism of the BCC lattices in respect to different aspect ratios were found to be consistent at three distinct relative densities: 6%, 10% and 20%. The stiffening mechanism of the BCC lattice with decreasing aspect ratio was also verified for a

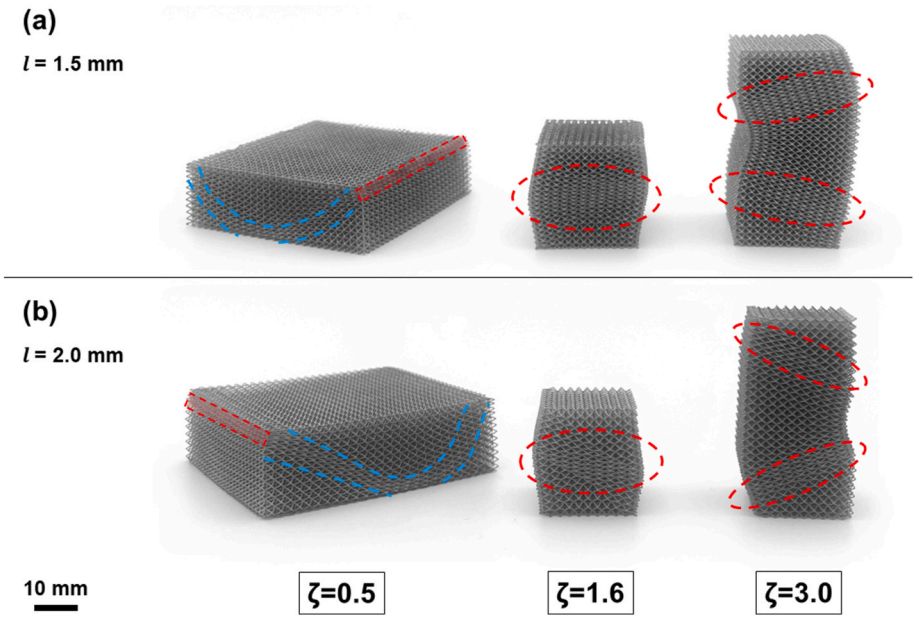

Fig. 8. Images of BCC lattices of different aspect ratios after quasi-static compression. Depicted specimens were made using unit cells with an edge length of (a) 1.5 mm or (b) 2.0 mm. Red circles indicate locally collapsed regions in the specimens, blue curved lines denote the generated shear bands. (For interpretation of the references to colour in this figure legend, the reader is referred to the Web version of this article.)

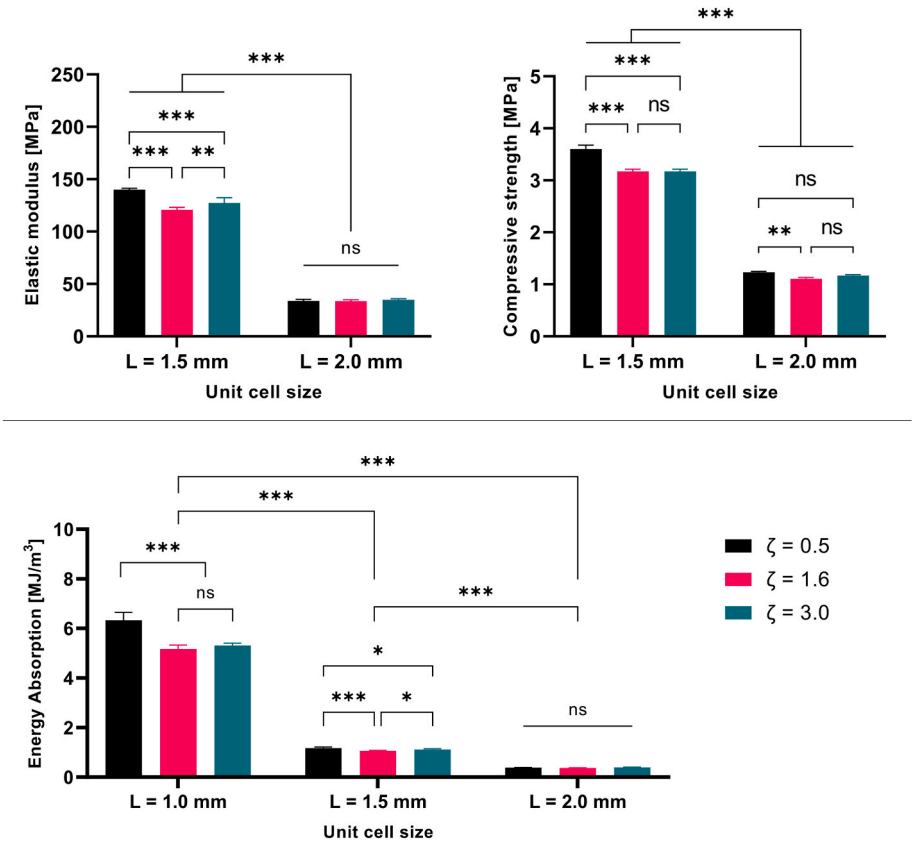

Fig. 9. Measurements of the elastic modulus E, compressive proof strength and energy absorption for different unit cell sizes of the BCC lattice. Statistical results are summarised with more detail in Tables S12-S14 in Supplementary materials.

relative density of 10%, but not in the case of 6% relative density. Thus, it seems that the effect of aspect ratio may attenuate for lattices with very low relative density.

Yield and compressive strength were found to be less impacted by aspect ratio, however in all cases their measured values increased at the smallest aspect ratios. This was more apparent for the BCC and octet-truss lattices which exhibited higher energy absorption and plasticity, respectively. Our observations for the octet-truss lattices greatly align with previous findings for quasi-brittle materials, such as metallic glasses, that also fail through shear band formation (Kechagias et al., 2022; Leary et al., 2018). From a thermo-mechanical perspective, higher post-yield softening (stress-drop) and lower plasticity has been linked to the larger elastic energy release for larger height or aspect ratio (Liu et al., 2011; Sha et al., 2014). This causes shear bands in high aspect ratio specimens to propagate rapidly leading to abruption; however, in low aspect ratio specimens, multiple dispersed shear bands propagate slowly and do no connect to form a catastrophic crack. The latter may not have made all low ζ lattices stiffer, but it made lattices able to withstand larger compression forces prior to failure.

This study verified that lattices' mechanical properties are constant for aspect ratio between 1 and 2 as suggested by international testing standards, however they can vastly differ outside this region. The different trends of convergence in stiffness, strength and energy absorption for different lattice types support the notion that extended mechanical characterisation should be done prior to designing parts whose geometry fall outside this aspect ratio.

4.2. Addressing challenges in mechanical testing of additively manufactured lattices

Variance in measured mechanical properties of cellular materials can be a product of manufacturing repeatability, specimen preparation, and testing protocols (Ashby et al., 2001). Several factors were considered in this regard. Firstly, specimens of same topology were fabricated in the same batches and same build direction to minimize the variance associated with the additive manufacturing process. Hence, only the properties of specimens with the same topology were statistically assessed. Secondly, the periodic lattices were designed with cubic unit cells so that no aspect ratio ($\zeta \neq 1$) would be favoured due to unit cell shape (Wallach and Gibson, 2001). Lastly, lattices were not printed attached to solid substrates/caps (Ashby et al., 2001) to avoid constraining struts' deformation.

Additively manufactured lattices are known to manifest several structural defects. Waviness and deviation of strut thickness in respect to build angle has previously shown to affect the failure mode and measured mechanical properties of lattice structures (Liu et al., 2017). While these phenomena cannot entirely be eliminated, tested lattices were built with consistent strut thickness and surface roughness regardless of strut angle, strut length and topology. Enclosed porosity is also known to affect the elastic properties of additively manufactured parts (Garlea et al., 2019). While this may be primarily apparent to solid parts, lattices in this study were fabricated with relatively thin struts (Ø230 μm) using low laser power (50 W) leading to near zero enclosed porosity as previously found in (Ghouse et al., 2017; Garlea et al., 2019).

Overall, the coefficient of variance of measured values was between 1% and 10% which is in line with foreseen ranges for measured stiffness and strength in foams and lattices (Ashby et al., 2001), demonstrating high consistency in the testing procedure. In the first part of the study, both the Z8 stochastic and the BCC lattices achieved converged mechanical properties regardless of the size of the tested specimens. In addition, lattices of the same topology demonstrated similar failure patterns for fixed aspect ratio. A minimum of 10 unit cells were used to form the edges in the periodic lattices, and the average pore size in all lattices was more than 10 times higher than specimens' smallest edge.

All the above inform that specimens were large enough to capture "bulk" material properties with minimal influence by structural defects.

4.3. Limitations and considerations for future work

This study exhibits several limitations that are worth discussing to guide future works.

Four widely used lattice topologies were tested with different relative densities (ranging from 6% to 30%), specimen geometry (cylindrical versus prismatic) and micro-architectures (stochastic versus periodic). Each topology demonstrated either a bend or stretch dominated micro-deformation mode, which is known to be independent of relative density and strut thickness-to-length ratio for fixed base material (Kechagias et al., 2022; Gümrük and Mines, 2013; Dong et al., 2015). Yet, different base materials have been shown to induce different failure modes for the same lattice designs due to their intrinsic ductile or brittle natural (Ghouse et al., 2018). For example, the bend-dominated BCC has been shown to fracture mainly through shear banding when made of the brittle Ti-6Al-4V (Lin et al., 2023), counter to what is observed for the pure titanium BCC lattices here. Nevertheless, the stiffening of our BCC lattices with decreasing aspect ratio agrees with previous computational data for bend-dominated lattices (Peng et al., 2022; Yang et al., 2019) using Ti-6Al-4V. Although this primarily verifies that the stiffening at low aspect ratios applies to bend-dominated structures, validation and global extension to other material types is left for future work.

Relative density was also found to influence the effect of aspect ratio on the mechanical properties of the BCC lattices. A future investigation for a wider range of relative densities, using additional topologies, will further enrich our knowledge regarding the effect of aspect ratio. In this case, however, a more rigorous analysis for the interplay of structural defects on the mechanical response may be necessary.

DIC was used to capture strain accumulation during the compression testing. 2D DIC was unable to capture out-of-plane deformation of external surfaces for the varying geometries. However, DIC was only used as a means of assessing the dominant deformation patterns of the different structures during compression testing. Due to the nature of compression testing, some strut features were not tracked in the later stages of plastic deformation – after cells fracture or densification. Nevertheless, the patterns necessary to understand the deformation were present in the early stages of plastic deformation (plateau region). Volumetric characterisation techniques, such as Digital Volume Correlation (Boniotti et al., 2022), can surpass current limitations and enable the calculation of deformation in multiple directions and properties such as Poisson ratio, shear and bulk modulus.

5. Conclusion

Specimen's aspect ratio and the stretch or bend dominated topology alters the measured mechanical properties of lattice structures. Stiffness is highly affected by aspect ratio and topology owing to different induced failure patterns. A layer-by-layer collapse leading to densification was observed in bend-dominated lattices, while failure through the formation of localised shear bands was observed in the stretch-dominated lattices. By testing lattices of different topologies, it was found that stretch-dominated lattices become stiffer for increasing aspect ratio, while bend-dominated lattices become stiffer for decreasing aspect ratio. Extended mechanical testing showed that convergence of stiffness values was achieved for $\zeta \leq 2$ in the stochastic and for $\zeta \geq 1$ in the BCC lattices. Engineering components that incorporate lattice structures with low or high aspect ratio should derive mechanical properties from similar aspect ratio test coupons.

CRediT authorship contribution statement

Stylianos Kechagias: Conceptualization, Formal analysis, Investigation, Methodology, Visualization, Writing – original draft. **Kabelan J. Karunaseelan:** Methodology, Software, Visualization, Writing – review & editing. **Reece N. Oosterbeek:** Methodology, Writing – review & editing. **Jonathan R.T. Jeffers:** Funding acquisition, Supervision, Writing – review & editing.

Declaration of competing interest

The authors declare that they have no known competing financial interests or personal relationships that could have appeared to influence the work reported in this paper.

Data availability

Data will be made available on request.

Acknowledgement

This work was funded by the National Institute for Health Research (NIHR300013) and the Engineering and Physical Sciences Research Council (EP/R042721/1). The authors wish to gratefully acknowledge Mr Tony Willis and Mr Ethan Lin from the Research Divisional Workshop of Imperial College London for the preparation of specimens.

Appendix A. Supplementary data

Supplementary data to this article can be found online at https://doi.org/10.1016/j.mechmat.2024.104944.

References

American Society for Testing and Materials, 2000. ASTM D1621 – Standard Test Method for Compressive Properties of Rigid Cellular Plastics.

Andrews, E.W., Gioux, G., Onck, P., Gibson, L.J., 2001. Size effects in ductile cellular solids. Part II: experimental results. Int. J. Mech. Sci. 43, 701–713. https://doi.org/10.1016/S0020-7403(00)00043-6.

Ang, B.L.S., Tan, Y.J., Ng, Y.J.P., Ong, S.H.F., Yap, S.Y., Gwee, S.X., Chou, S.M., Poh, C. L., Yew, K.S., 2012. The effect of specimen geometry on the mechanical behavior of trabecular bone specimens. In: Solid State Phenomena. Trans Tech Publications Ltd, pp. 129–132. https://doi.org/10.4028/www.scientific.net/SSP.185.129.

Ashby, M.F., 2006. The properties of foams and lattices. Phil. Trans. Math. Phys. Eng. Sci. 364, 15–30. https://doi.org/10.1098/rsta.2005.1678.

Ashby, M.F., Evans, A.G., Fleck, N.A., Gibson, L.J., Hutchinson, J.W., Wadley, H.N.G., 2001. Metal Foams: A Design Guide. Butterworth-Heinemann.

Boniotti, L., Dancette, S., Gavazzoni, M., Lachambre, J., Buffiere, J.Y., Foletti, S., 2022. Experimental and numerical investigation on fatigue damage in micro-lattice materials by Digital Volume Correlation and μCT-based finite element models. Eng. Fract. Mech. 266, 108370 https://doi.org/10.1016/J.ENGFRACMECH.2022.108370.

Bühring, J., Soika, J., Schirp-Schoenen, M., Schröder, K.U., 2022. Elastic Axial Stiffness Properties of Lattice Structures: Analytical Approach and Experimental Validation for Bcc and F2cc,z Unit Cells, Mechanics of Advanced Materials and Structures. https://doi.org/10.1080/15376494.2022.2139027.

Burge, T.A., Munford, M.J., Kechagias, S., Jeffers, J.R.T., Myant, C.W., 2023. Automating the customization of stiffness-matched knee implants using machine learning techniques. Int. J. Adv. Des. Manuf. Technol. https://doi.org/10.1007/s00170-023-11357-6.

Contreras Raggio, J.I., Arancibia, C.T., Millán, C., Ploeg, H.L., Aiyangar, A., Vivanco, J.F., 2022. Height-to-Diameter ratio and porosity strongly influence bulk compressive mechanical properties of 3D-printed polymer scaffolds. Polymers 14. https://doi.org/10.3390/polym14225017.

Cortis, G., Mileti, I., Nalli, F., Palermo, E., Cortese, L., 2022. Additive manufacturing structural redesign of hip prostheses for stress-shielding reduction and improved functionality and safety. Mech. Mater. 165, 104173 https://doi.org/10.1016/J.MECHMAT.2021.104173.

Deshpande, V.S., Ashby, M.F., Fleck, N.A., 2001. Foam topology: bending versus stretching dominated architectures. Acta Mater. 49, 1035–1040. https://doi.org/10.1016/S1359-6454(00)00379-7.

Dong, L., Deshpande, V., Wadley, H., 2015. Mechanical response of Ti–6Al–4V octet-truss lattice structures. Int. J. Solid Struct. 60–61. https://doi.org/10.1016/J.IJSOLSTR.2015.02.020, 107–124.

Findeisen, C., Hohe, J., Kadic, M., Gumbsch, P., 2017. Characteristics of mechanical metamaterials based on buckling elements. J. Mech. Phys. Solid. 102, 151–164. https://doi.org/10.1016/j.jmps.2017.02.011.

Garlea, E., Choo, H., Sluss, C.C., Koehler, M.R., Bridges, R.L., Xiao, X., Ren, Y., Jared, B. H., 2019. Variation of elastic mechanical properties with texture, porosity, and defect characteristics in laser powder bed fusion 316L stainless steel. Mater. Sci. Eng., A 763, 138032. https://doi.org/10.1016/J.MSEA.2019.138032.

Ghouse, S., Babu, S., Van Arkel, R.J., Nai, K., Hooper, P.A., Jeffers, J.R.T., 2017. The influence of laser parameters and scanning strategies on the mechanical properties of a stochastic porous material. Mater. Des. 131 https://doi.org/10.1016/j.matdes.2017.06.041.

Ghouse, S., Babu, S., Nai, K., Hooper, P.A., Jeffers, J.R.T., 2018. The influence of laser parameters, scanning strategies and material on the fatigue strength of a stochastic porous structure. Addit. Manuf. 22, 290–301. https://doi.org/10.1016/j.addma.2018.05.024.

Gümrük, R., Mines, R.A.W., 2013. Compressive behaviour of stainless steel micro-lattice structures. Int. J. Mech. Sci. 68, 125–139. https://doi.org/10.1016/j.ijmecsci.2013.01.006.

Guo, Y., Chen, C., Wang, Q., Liu, M., 2021. Effects of reuse on the properties of tantalum powders and tantalum parts additively manufactured by electron beam powder bed fusion. Mater. Res. Express 8. https://doi.org/10.1088/2053-1591/abf60e.

Hildebrand, T., Ruegsegger, P., 1997. A new method for the model-independent assessment of thickness in three-dimensional images. J. Microsc. 185, 67–75. https://doi.org/10.1046/j.1365-2818.1997.1340694.x.

Hossain, U., Ghouse, S., Nai, K., Jeffers, J.R., 2021. Controlling and testing anisotropy in additively manufactured stochastic structures. Addit. Manuf. 39 https://doi.org/10.1016/j.addma.2021.101849.

International Organization for Standardization, 2011. ISO 13314:2011 Mechanical Testing of Metals – Ductility Testing – Compression Test for Porous and Cellular Metals.

Keaveny, T.M., Borchers, R.E., Gibson, L.J., Hayes, W.C., 1993. Theoretical analysis of the experimental artifact in trabecular bone compressive modulus. J. Biomech. 26, 599–607. https://doi.org/10.1016/0021-9290(93)90021-6.

Kechagias, S., Oosterbeek, R.N., Munford, M.J., Ghouse, S., Jeffers, J.R.T., 2022. Controlling the mechanical behaviour of stochastic lattice structures: the key role of nodal connectivity. Addit. Manuf. 54, 102730 https://doi.org/10.1016/J.ADDMA.2022.102730.

Leary, M., Mazur, M., Williams, H., Yang, E., Alghamdi, A., Lozanovski, B., Zhang, X., Shidid, D., Farahbod-Sternahl, L., Witt, G., Kelbassa, I., Choong, P., Qian, M., Brandt, M., 2018. Inconel 625 lattice structures manufactured by selective laser melting (SLM): mechanical properties, deformation and failure modes. Mater. Des. 157, 179–199. https://doi.org/10.1016/j.matdes.2018.06.010.

Lei, H., Li, C., Zhang, X., Wang, P., Zhou, H., Zhao, Z., Fang, D., 2021. Deformation behavior of heterogeneous multi-morphology lattice core hybrid structures. Addit. Manuf. 37 https://doi.org/10.1016/j.addma.2020.101674.

Lin, Y., Shi, W., Li, J., Liu, Y., Liu, S., Li, J., 2023. Evaluation of mechanical properties of Ti–6Al–4V BCC lattice structure with different density gradient variations prepared by L-PBF. Mater. Sci. Eng. 872. https://doi.org/10.1016/j.msea.2023.144986.

Linde, F., Hvid, I., Madsen, F., 1992. The effect of specimen geometry on the mechanical behaviour of trabecular bone specimens. J. Biomech. 25, 359–368. https://doi.org/10.1016/0021-9290(92)90255-Y.

Liu, Z., Li, R., Wang, G., Wu, S., Lu, X., Zhang, T., 2011. Quasi phase transition model of shear bands in metallic glasses. Acta Mater. 59, 7416–7424. https://doi.org/10.1016/J.ACTAMAT.2011.08.002.

Liu, L., Kamm, P., García-Moreno, F., Banhart, J., Pasini, D., 2017. Elastic and failure response of imperfect three-dimensional metallic lattices: the role of geometric defects induced by Selective Laser Melting. J. Mech. Phys. Solid. 107, 160–184. https://doi.org/10.1016/J.JMPS.2017.07.003.

Liu, F., Mao, Z., Zhang, P., Zhang, D.Z., Jiang, J., Ma, Z., 2018. Functionally graded porous scaffolds in multiple patterns: new design method, physical and mechanical properties. Mater. Des. 160, 849–860. https://doi.org/10.1016/J.MATDES.2018.09.053.

Maconachie, T., Leary, M., Lozanovski, B., Zhang, X., Qian, M., Faruque, O., Brandt, M., 2019. SLM lattice structures: properties, performance, applications and challenges. Mater. Des. 183, 108137 https://doi.org/10.1016/j.matdes.2019.108137.

Nazarian, A., Stauber, M., Müller, R., 2005. Design and implementation of a novel mechanical testing system for cellular solids. J. Biomed. Mater. Res. B Appl. Biomater. 73, 400–411. https://doi.org/10.1002/jbm.b.30232.

Oosterbeek, R.N., Jeffers, J.R.T., 2022. StrutSurf: a tool for analysis of strut morphology and surface roughness in additively manufactured lattices. SoftwareX 18, 101043. https://doi.org/10.1016/J.SOFTX.2022.101043.

Pehlivan, E., Roudnicka, M., Dzugan, J., Koukolikova, M., Králík, V., Seifi, M., Lewandowski, J.J., Dalibor, D., Daniel, M., 2020. Effects of build orientation and sample geometry on the mechanical response of miniature CP-Ti Grade 2 strut samples manufactured by laser powder bed fusion. Addit. Manuf. 35, 101403 https://doi.org/10.1016/J.ADDMA.2020.101403.

Peng, X., Huang, Q., Zhang, G., Li, J., Zhang, X., Lu, Y., Jin, Z., 2022. Compensating the anisotropic mechanical properties of electron beam melting-based Gyroid scaffolds using structural design. Int. J. Mech. Sci. 226, 107442 https://doi.org/10.1016/J.IJMECSCI.2022.107442.

Pham, R.D., Hütter, G., 2021. Influence of topology and porosity on size effects in stripes of cellular material with honeycomb structure under shear, tension and bending. Mech. Mater. 154, 103727 https://doi.org/10.1016/J.MECHMAT.2020.103727.

Qi, D., Yu, H., Liu, M., Huang, H., Xu, S., Xia, Y., Qian, G., Wu, W., 2019. Mechanical behaviors of SLM additive manufactured octet-truss and truncated-octahedron lattice structures with uniform and taper beams. Int. J. Mech. Sci. 163, 105091 https://doi.org/10.1016/J.IJMECSCI.2019.105091.

Sha, Z.D., He, L.C., Xu, S., Pei, Q.X., Liu, Z.S., Zhang, Y.W., Wang, T.J., 2014. Effect of aspect ratio on the mechanical properties of metallic glasses. Scripta Mater. 93, 36–39. https://doi.org/10.1016/J.SCRIPTAMAT.2014.08.025.

Tekoglu, C., Gibson, L.J., Pardoen, T., Onck, P.R., 2011. Size effects in foams: experiments and modeling. Prog. Mater. Sci. 56, 109–138. https://doi.org/10.1016/J.PMATSCI.2010.06.001.

Thomson, R.C., Yaszemski, M.J., Powers, J.M., Mikos, A.G., 1995. Fabrication of biodegradable polymer scaffolds to engineer trabecular bone. J. Biomater. Sci. Polym. Ed. 7, 23–38. https://doi.org/10.1163/156856295X00805.

Vangelatos, Z., Komvopoulos, K., Grigoropoulos, C.P., 2020. Regulating the mechanical behavior of metamaterial microlattices by tactical structure modification. J. Mech. Phys. Solid. 144, 104112 https://doi.org/10.1016/j.jmps.2020.104112.

Vesenjak, M., Veyhl, C., Fiedler, T., 2012. Analysis of anisotropy and strain rate sensitivity of open-cell metal foam. Mater. Sci. Eng., A 541, 105–109. https://doi.org/10.1016/J.MSEA.2012.02.010.

Wallach, J.C., Gibson, L.J., 2001. Mechanical behavior of a three-dimensional truss material. Int. J. Solid Struct. 38, 7181–7196. https://doi.org/10.1016/S0020-7683(00)00400-5.

Xia, X., Zhao, W., Wei, Z., Wang, Z., 2012. Effects of specimen aspect ratio on the compressive properties of Mg alloy foam. Mater. Des. 42, 32–36. https://doi.org/10.1016/J.MATDES.2012.05.011.

Yang, H., Ma, L., 2019. Multi-stable mechanical metamaterials by elastic buckling instability. J. Mater. Sci. 54, 3509–3526. https://doi.org/10.1007/s10853-018-3065-y.

Yang, Y., Shan, M., Zhao, L., Qi, D., Zhang, J., 2019. Multiple strut-deformation patterns based analytical elastic modulus of sandwich BCC lattices. Mater. Des. 181, 107916 https://doi.org/10.1016/J.MATDES.2019.107916.

Yoder, M., Thompson, L., Summers, J., 2018. Size effects in lattice structures and a comparison to micropolar elasticity. Int. J. Solid Struct. 143, 245–261. https://doi.org/10.1016/j.ijsolstr.2018.03.013.

Zadpoor, A.A., 2019. Mechanical performance of additively manufactured meta-biomaterials. Acta Biomater. 85, 41–59. https://doi.org/10.1016/j.actbio.2018.12.038.

Zhang, W., Zhao, J., Tan, Y., Gao, Y., Wang, J., Geng, X., 2022. Study on the shear modulus based equivalent homogenization methods of multi-layer BCC lattice sandwich. Materials 15. https://doi.org/10.3390/ma15041341.

Zupan, M., Deshpande, V.S., Fleck, N.A., 2004. The out-of-plane compressive behaviour of woven-core sandwich plates. Eur. J. Mech. Solid. 23, 411–421. https://doi.org/10.1016/j.euromechsol.2004.01.007.